Non-concentric textured closed surface for huge local field enhancement

2017 J. Opt. 19 015005

(http://iopscience.iop.org/2040-8986/19/1/015005)

IOP Publishing Journal of Optics
J. Opt. 19 (2017) 015005 (6pp) doi:10.1088/2040-8986/19/1/015005

Non-concentric textured closed surface for huge local field enhancement

Bingzheng Xu[1,2], Zhuo Li[1,3,4,6], Liangliang Liu[1], Hengyi Sun[1], Chen Chen[1], Jia Xu[1], Tao Yuan[5] and Changqing Gu[1]

[1] Key Laboratory of Radar Imaging and Microwave Photonics, Ministry of Education, College of Electronic and Information Engineering, Nanjing University of Aeronautics and Astronautics, Nanjing, 211106, People's Republic of China
[2] Department of Electrical and Computer Engineering, National University of Singapore, 117576, Singapore
[3] State Key Laboratory of Millimeter Waves, Southeast University, Nanjing, 210096, People's Republic of China
[4] Department of Physics, College of Liberal Arts and Sciences, Arizona State University, 871504, USA
[5] ATR National Key Lab. of Defense Technology, Shenzhen University, Shenzhen, 518060, People's Republic of China

E-mail: lizhuo@nuaa.edu.cn

Received 6 July 2016, revised 11 November 2016
Accepted for publication 17 November 2016
Published 15 December 2016

Abstract

It has been demonstrated that textured closed surfaces are good platforms to support spoof localized surface plasmons with great field confinement and enhancement. Here, we propose a non-concentric textured closed structure to significantly increase the level of field confinement and enhancement. By properly texturing the closed surface with gradient-depth grooves, we show that the incoming electromagnetic waves can be highly confined and focused at the deepest groove on the closed surface. Moreover, we find that the field enhancement factor of this structure is quite sensitive to the polarization angle of the incident wave, which can find potential applications in polarization sensors and energy harvesting devices at microwave and terahertz frequencies.

Keywords: surface plasmons, subwavelength structures, surface waves

(Some figures may appear in colour only in the online journal)

1. Introduction

Arising around metallic nanoparticles, localized surface plasmons (LSPs) are non-propagation excitations of the conduction electrons in metallic nanostructures coupled to the electromagnetic (EM) field at visible and near-infrared regions [1, 2]. Nowadays, LSPs are excellent candidates for surface-enhanced Raman scattering [3], plasmonic antennae [4], nanolasers [5], sensors [6], etc. Recently, a metal cylinder of crescent-shaped cross section with kissing crescent tips has been demonstrated to hold promise for achieving broadband harvesting of light [7]. However, as subwavelength confinement of surface plasmons relies on the penetration of the EM field into the metal, almost all investigations and promising applications of LSPs have been limited to the infrared and visible spectrum [8]. A pioneering work to safely transfer nearly all the amazing properties of LSPs to lower frequencies has been carried out in [9], in which a two dimensional (2D) periodically textured metallic cylinder was proved to be able to support spoof localized surface plasmons (SLSPs), and two infinitely close 3D textured cylinders could achieve great field enhancement. After this new concept was reported, the existence of SLSPs has been experimentally verified on an ultrathin textured metallic disk [10] and a series of studies concerning SLSPs has been presented in recent years [11–20]. Spoof surface plasmon polaritons (SSPPs) have also attracted a great deal of interest since Pendry *et al* [21] show that even perfect electric conducting surfaces can sustain modes

[6] Author to whom any correspondence should be addressed.

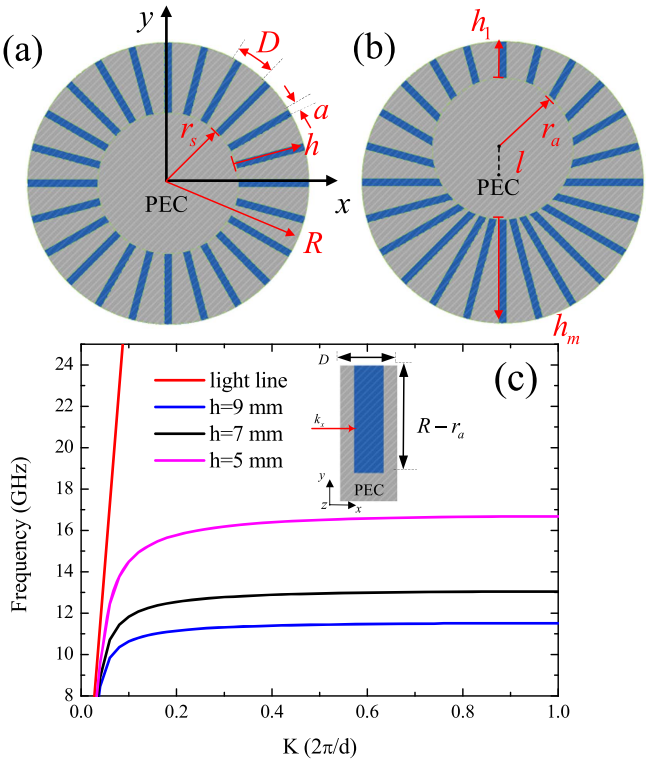

Figure 1. (a) A 2D perfect electric conducor (PEC) textured cylinder with inner and outer radii r_s and R, periodicity D, and groove width a. (b) The proposed non-concentric 2D textured cylinder with gradient groove depths from h_1 to h_m and inner radius r_a. (c) The dispersion property of the corrugated metallic unit with different groove depths varying from 5 mm to 9 mm with a step of 2 mm, in which the red curve is the light line.

resembling surface plasmon polaritons at optical frequencies [21–24]. Guiding and focusing surface plasmon polaritons are also feasible in helical grooves decorated on cylindrical metal wires [25–27].

In this paper, we propose a simple scheme to achieve SSPP focusing and field enhancement on a 2D non-concentric metallic closed surface by texturing it with gradient depths grooves so that the incoming waves can be focused at the surface of the deepest depth grooves, leading to huge local field enhancement compared with the traditional concentric structure. In addition, we find that the field enhancement factor (FEF) of the non-concentric 3D structure is very sensitive to the polarization angle of the incident wave, which can find potential applications in sensing, spectroscopy, and near-field imaging in the microwave and terahertz (THz) frequencies.

First, we start by revisiting the 2D closed textured surface [9] shown in figure 1(a), which is corrugated with N periodic grooves with outer and inner radii R and r_s. The height and width of the radial grooves are $h = R - r_s$ and a. The proposed non-concentric 2D textured closed surface is shown in figure 1(b) with the inner cylinder not being in the center of the whole structure. The distance between the center position of the inner and outer cylinders is set as l. The grooves' depth h smoothly increases from h_1 to h_m along the peripheral direction on both sides. Actually, each curve in figure 1(c) obtained by the commercial software COMSOL Multiphysics corresponds to the dispersion relation of the surface EM mode that propagates along a flat perfect electric conducting surface corrugated with periodical grooves of a certain depth. Thus, we can pick up one unit cell from figure 1(b) and put it into COMSOL Multiphysics, in which the boundary conditions applied at four sides are shown in the inset of figure 1(c). As the groove depth increases from $h_1 = 5$ mm to $h_m = 9$ mm, the asymptotic frequency of the dispersion curve becomes lower and the curve deviates more from the light line, which shows a higher confinement level of SSPPs.

In order to probe the plasmonic resonances, we consider a transverse magnetic (TM)-polarized incident plane wave (electric field $\overrightarrow{E}$ pointing along the x direction and magnetic field $\overrightarrow{H}$ pointing along the z direction) propagating along the y axis. Actually, in COMSOL Multiphysics [1], the scattering cross section of an object in the 2D case can be obtained by a 1D line integral of the scattered field's power density along the whole scattering boundary, which is the interface between the perfectly matched layer and the far field domain. Thus, we can set the incident plane wave as background excitations and calculate the normalized scattering cross section by the real scattering cross section divided by the diameter of the structure.

The geometrical parameters of the non-concentric structure are also set to be $R = 10$ mm, $N = 120$, and $a = D/2$. The material in the groove is set to be air $\epsilon_r = 1$. We first study how SLSP resonances are affected by varying the inner radius r_a with fixed $l = 2$ mm. The normalized scattering cross section spectra for a conventional concentric structure ($h = 9$, 7, 5 mm and $r_s = 1$, 3, 5 mm) and a specified non-centric one ($l = 2$ mm, $r_a = 3$ mm, $h_1 = 5$ mm, and $h_m = 9$ mm) are shown in figures 2(a) and (b). The normalized scattering cross section curves shown in figure 2 consist of multiple peaks which are related to the resonant behavior of the two types of structures. The conventional concentric structure has uniform grooves with depth that the three peaks (M_1, M_2, and M_3) correspond to the hexa-, octo-, and decapolar resonances [9]. With decreasing h, the three peaks M_1–M_3 significantly blueshift due to the increase of the asymptotic frequency ($\omega_a = \pi c/2h$) of the corresponding SSPPs that would propagate along the textured surface with the same depth grooves. However, it can be observed that the normalized scattering cross section curve of the non-concentric structure exhibits a series of peaks corresponding to the gradient grooves. And it can been seen that there is a series of sharp peaks on the high frequency slope of the broad peak. The non-concentric structure has gradient grooves, we think the series of the sharp peaks are generated by the gradient grooves. And the sharp peaks on the high frequency slope are generated by the shallow grooves. As shown in the right panels in figure 2, distributions of the electric field amplitudes $|\vec{E}|$ at resonance frequencies A_1, A_2, and A_3 are quite different from those of conventional concentric structure (M_1, M_2, M_3), so that the non-concentric structure tends to confine the fields gradually and focus the energy at the surface of the deepest groove. Thus, it is of great interest to study field confinement

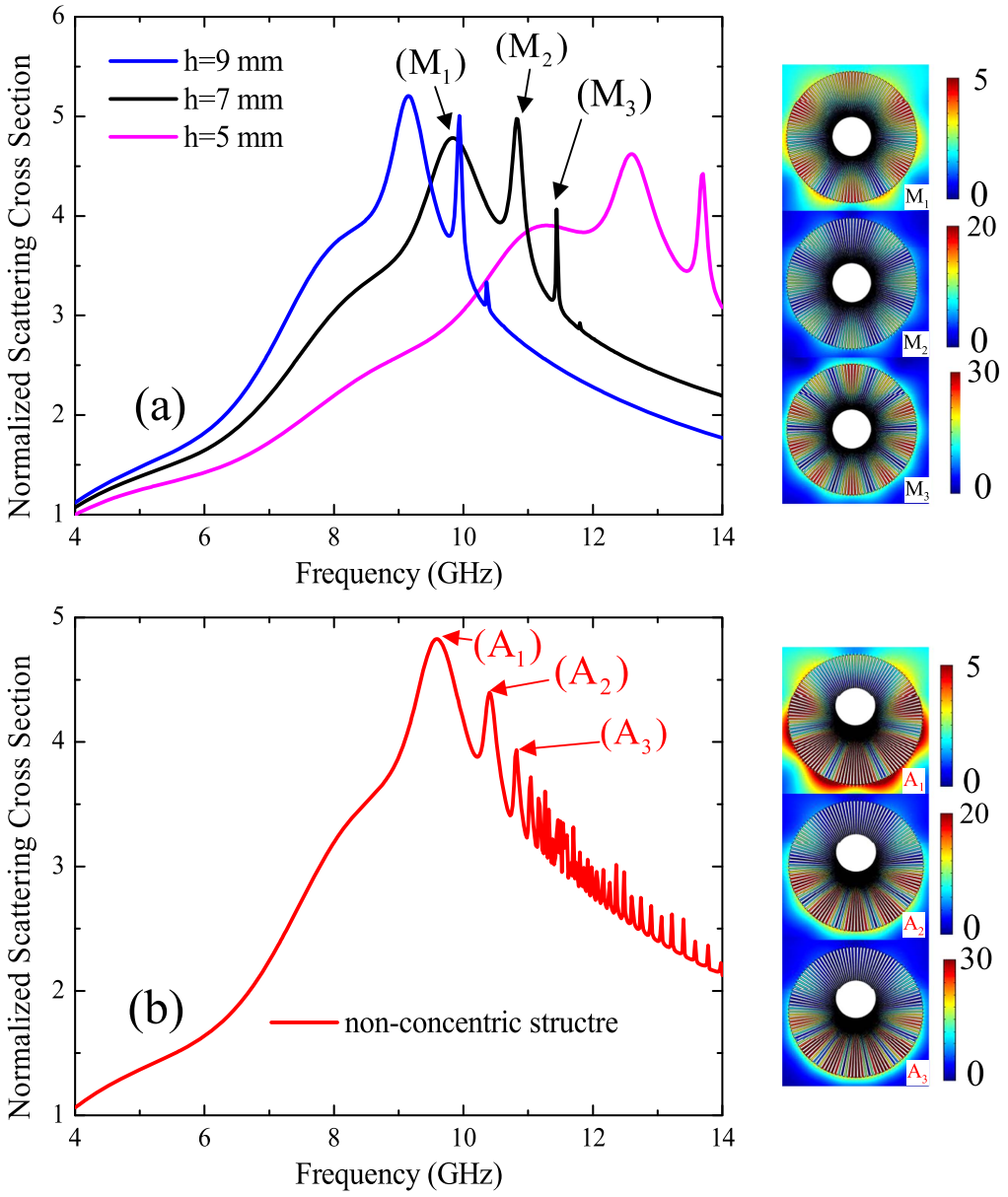

Figure 2. Calculated normalized scattering cross section curves of (a) conventional concentric structure with $h = 9$, 7, and 5 mm and $r_s = 1$, 3, 5 mm, and (b) non-concentric structure with $l = 2$ mm, $r_a = 3$ mm. For the conventional concentric structure, the marked peaks M_1, M_2, and M_3 correspond to the hexa-, octo-, and decapolar resonances when $r_s = 3$ mm. For the non-concentric model, the marked peaks A_1, A_2, and A_3 correspond to the first three resonances when $r_a = 3$ mm. And the right panels show the distributions of the electric field amplitudes $|\vec{E}|$ at these resonances peaks.

and enhancement of the non-concentric structure with different dimensions.

Next, we analyze the amplitude $|E_x|$ around the non-concentric ($h_1 = 5$ mm, $h_m = 9$ mm) and concentric ($h = 7$ mm) closed surfaces. The electric field of the incident x-polarized plane wave has the form $\vec{E_0} = \vec{e}_x E_0 e^{jk_0 y}$ and $E_0 = 1$ V/m. To demonstrate the field focusing characteristic quantitatively, one probe is set right below the closed surface of the structure in the right panels of figure 3. And we choose the ratio of the amplitude of the x component of scattered electric field $|E_x|$ to E_0 as the FEF. In the whole spectrum, the FEF for the conventional concentric structure at the probe denoted by the red solid line is not higher than 10. For the non-concentric structure, however, the FEF fluctuates greatly and exceeds 30 from 10 GHz to 11.5 GHz and even reaches 300 at 11.5 GHz. It is worth noting that the FEF drops down to zero sharply above 11.5 GHz, which is actually the asymptotic frequency of the SSPPs that would propagate along a periodically corrugated surface with the deepest groove of depth $h = 9$ mm. Distributions of E_x along the circumferential direction for the non-concentric structure at 11.5 GHz are shown in the inset in figure 3, from which we can clearly observe that with increasing groove depth, the electric fields confine more on the corrugated surface and finally focus at the deepest groove below the asymptotic frequency 11.5 GHz. One probe is set right below the closed

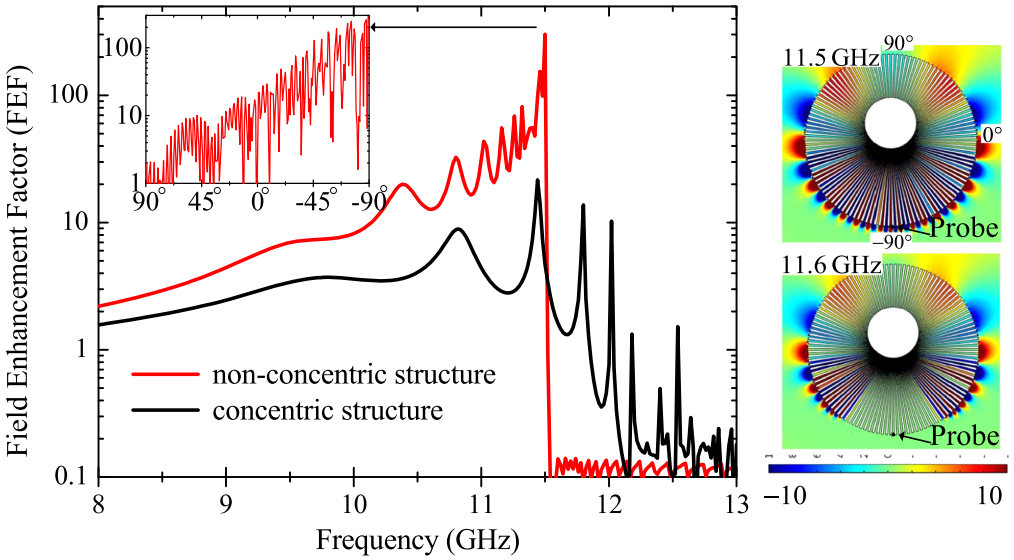

Figure 3. FEF spectra for the concentric (black) and non-concentric (red) structures. Distributions of E_x along the circumferential direction (from 90° to −90°) for the non-concentric structure at 11.5 GHz are shown as the inset in figure 3. The right two panels show E_x at 11.5 and 11.6 GHz for the non-concentric structure.

Table 1. Parameters of the non-concentric structure in figure 4(a).

l (mm)	h_1(mm)	h_m(mm)
4	0	8
3	1	7
2	2	6

surface of the non-concentric and concentric structure, but the groove heights at the probe position are different for the two cases. For the non-concentric case, when the frequency exceeds 11.5 GHz, there is no energy distribution at this location, so a sharp cut-off occurs. In addition, the field distributions of the SLSP resonances for the non-concentric structure manifest a wavelength shortening phenomenon along the circumferential direction from the shallowest groove toward the deepest one in the whole spectrum, and are quite different from the concentric structure which only shows equal-spaced field distributions along the circumferential direction at discrete SLSP resonant peaks.

Furthermore, we study how field enhancement can be affected by the geometrical parameters of the non-concentric structure. We first examine the case when $r_a = 6$ mm, $R = 10$ mm, $a/D = 0.5$ are fixed and l is increased from 2 mm to 4 mm with a step of 1 mm, and the corresponding dimensions of h_1 and h_m are listed in table 1. As shown in figure 4(a), when $l = 4$ mm, the non-concentric structure has the largest FEF at 12 GHz (see the red solid curve). With decreasing l down to 2 mm, the frequency at which the largest FEF occurs exhibits a blueshift and the field enhancement factor peak value decreases, which means that a larger FEF peak value can be expected by enlarging the difference between the shallowest and deepest grooves.

Then, we fix $R = 10$ mm, $a/D = 0.5$, $l = 2$ mm, and decrease r_a from 6 mm to 3 mm with a step of 1 mm. The corresponding FEF curves are shown in figure 4(b), which indicate that, with decreasing r_a, the asymptote frequency of the dispersion curves decreases, and the FEF increases accordingly. We consider another case when $R = 10$ mm, $r_a = 3$ mm, and $l = 2$ mm are fixed and the ratio of groove width a to the period D is changed from 0.1 to 0.9 with a step of 0.2. It can be observed from figure 4(c) that with the decrease of a/D, the asymptotic frequency shifts from 11.4 to 11.6 GHz and a greater FEF is obtained with the curves becoming much smoother. Finally, we examine the FEF spectrum with different outer radius R when the parameters $r_a = 4$ mm, $a/D = 0.1$, and $l = 2$ mm are fixed. When the outer radius R increases from 9 mm to 11 mm, the deepest groove changes from 8 mm to 10 mm, leading to a decrease of the asymptotic frequency and increase of the FEF peak value, which can be observed in figure 4(d).

Up to now, we have analyzed the resonance characteristics and FEF of the 2D structure. It is of great interest and value to study whether the field enhancement effect can also be observed in 3D models. Figure 5 shows the FEF for the proposed 3D non-concentric structure when $a/D = 0.5$, $h_1 = 5$ mm, $h_m = 9$ mm, $N = 120$, and thickness $t_0 = 0.018$ mm. We focus on the sensitivity of the field enhancement to polarization angle of the incident plane wave, which propagates along the $-y$ direction and the amplitude of the incident electric field is set to 1 V/m. For clarity, the polarization angle θ is defined as the angle between the electric field vector and the $+x$ direction in the xz plane. To demonstrate the focusing characteristic quantitatively, one probe is set at the surface of the 3D structure as shown in figure 5, which is located 0.5 mm away from the structure and is vertical to the xy plane. Figure 5 shows the amplitudes of the electric field ($|\vec{E}|$) which is extracted from the probe with different θ. It can be observed that the amplitudes of the electric field show great sensitivity to the polarization angle θ of the incident wave and frequency. It is clear that the peak of

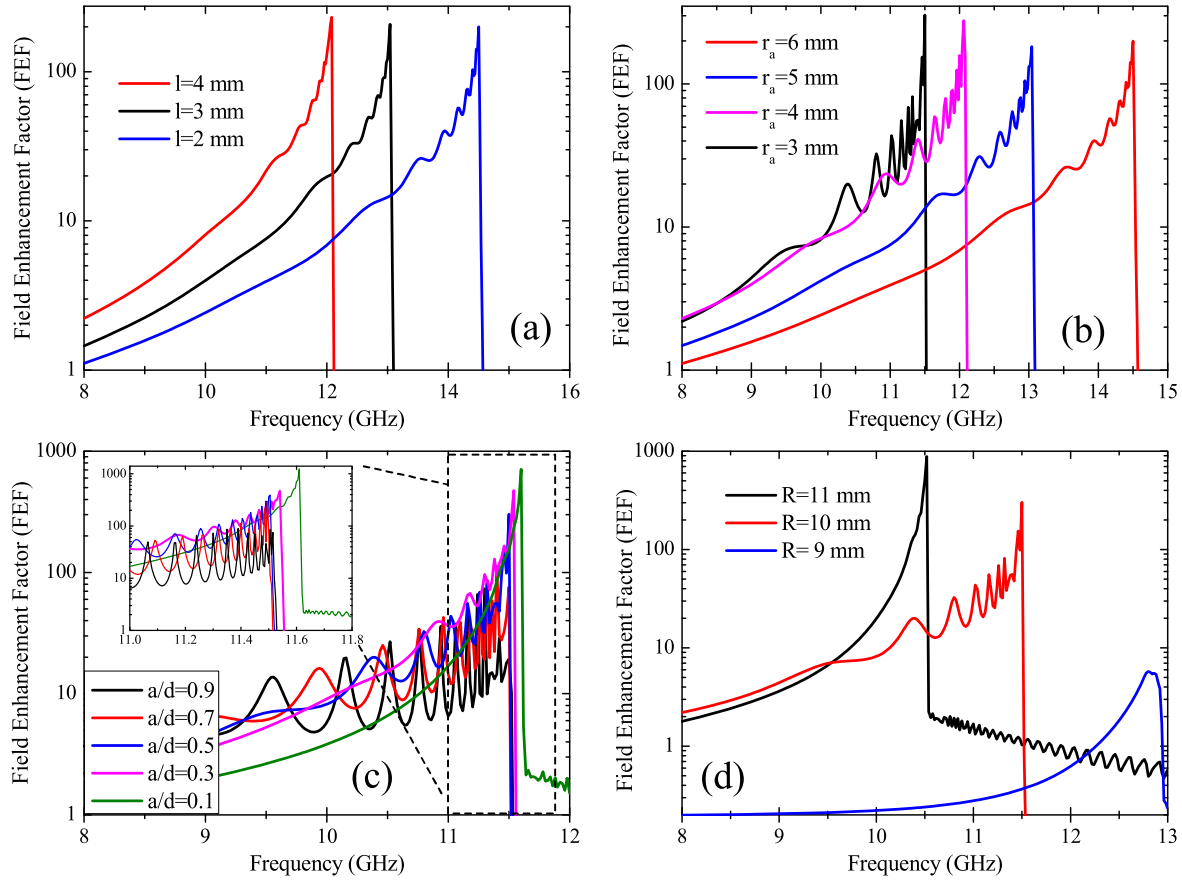

Figure 4. (a) FEF at the probe for different l, with the lattice constant fixed to $R = 10$ mm, $r_a = 6$ mm, $a/D = 0.5$; (b) FEF at the probe for different r_a, with the lattice constant fixed to $R = 10$ mm, $l = 2$ mm, $a/D = 0.5$; (c) FEF at the probe for different a/d, with the lattice constant fixed to $R = 10$ mm, $l = 2$ mm, $r_a = 3$ mm ; (d) FEF at the probe for different R, with the lattice constant fixed to $l = 2$ mm, $r_a = 4$ mm, $a/D = 0.1$.

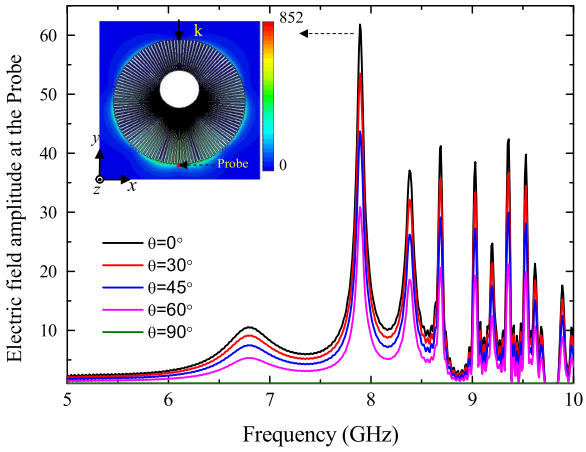

Figure 5. Electric field amplitudes $|\vec{E}|$ of the probe for the non-concentric structure with different polarization angles. The inset show the electric field amplitude distributions of the structure surface at the highest value at about 7.89 GHz when $\theta = 0°$.

the amplitudes of the electric field monotonically decreases with increasing incident polarization angle in the whole spectrum, which demonstrates that the x component of the incident electric fields contributes to the field enhancement effect. Thus, this phenomenon can be fully utilized to realize polarization sensors at microwave and THz frequencies.

Based on the SLSP, a broadband electromagnetic field enhancement is realized with non-concentric textured closed structure. Numerical simulations show that the FEF at the surface of the structure can reach at least one order of magnitude higher than that of the conventional concentric one. Moreover, we find that the non-concentric 3D structure is quite sensitive to polarization angle, which can find potential applications in polarization sensors and energy harvesting devices in the microwave and THz regimes.

Acknowledgments

This work was supported in part by the Natural Science Foundation of Jiangsu Province (BK20151480), in part by the Foundation of State Key Laboratory of Millimeter Waves, Southeast University, China, under Grant No. K201603, in part by the Funding of Jiangsu Innovation Program for Graduate Education under Grant No. KYLX_0276, in part by the priority academic program development of Jiangsu Higher Education Institutions, in part by the Fundamental Research Funds for the Central Universities(NS2016039), and in part by the China Scholarship Council (CSC).

References

[1] Oldenburg S J, Jackson J B, Westcott S L and Halas N J 1999 Infrared extinction properties of gold nanoshells *Appl. Phys. Lett.* **75** 2897–9

[2] Kreibig U and Vollmer M 2013 *Optical Properties of Metal Clusters* (Berlin: Springer)

[3] Li W Y, Camargo P H, Lu X M and Xia Y N 2008 Dimers of silver nanospheres: facile synthesis and their use as hot spots for surface-enhanced Raman scattering *Nano Lett.* **9** 485–90

[4] Cubukcu E, Kort E A, Crozier K B and Capasso F 2006 Plasmonic laser antenna *Appl. Phys. Lett.* **89** 093120

[5] Berini P and De Leon I 2012 Surface plasmon-polariton amplifiers and lasers *Nat. Photon.* **6** 16–24

[6] Anker J N, Hall W P, Lyandres O, Shah N C, Zhao J and Van Duyne R P 2008 Biosensing with plasmonic nanosensors *Nat. Mater.* **7** 442–53

[7] Aubry A, Lei D Y, Fernández-Domínguez A I, Sonnefraud Y, Maier S A and Pendry J B 2010 Plasmonic light-harvesting devices over the whole visible spectrum *Nano Lett.* **10** 2574–9

[8] Maier S A 2007 *Plasmonics: Fundamentals and Applications* (New York: Springer)

[9] Pors A, Moreno E, Martin-Moreno L, Pendry J B and Garcia-Vidal F J 2012 Localized spoof plasmons arise while texturing closed surfaces *Phys. Rev. Lett.* **108** 223905

[10] Shen X and Cui T J 2014 Ultrathin plasmonic metamaterial for spoof localized surface plasmons *Laser Photon. Rev.* **8** 137–45

[11] Huidobro P A, Shen X P, Cuerda J, Moreno E, Martin-Moreno L, Garcia-Vidal F J, Cui T J and Pendry J B 2014 Magnetic localized surface plasmons *Phys. Rev.* X **4** 021003

[12] Liao Z, Luo Y, Fernández-Domínguez A I, Shen X, Maier S A and Cui T J 2015 High-order localized spoof surface plasmon resonances and experimental verifications *Sci. Rep.* **5** 9590

[13] Li Z, Liu L L, Gu C Q, Ning P P, Xu B Z, Niu Z Y and Zhao Y J 2014 Multi-band localized spoof plasmons with texturing closed surfaces *Appl. Phys. Lett.* **104** 101603

[14] Li Z, Xu B Z, Gu C Q, Ning P P, Liu L L, Niu Z Y and Zhao Y J 2014 Localized spoof plasmons in closed textured cavities *Appl. Phys. Lett.* **104** 251601

[15] Xu B Z, Li Z, Gu C Q, Ning P P, Liu L L, Niu Z Y and Zhao Y J 2014 Multiband localized spoof plasmons in closed textured cavities *Appl. Opt.* **53** 6950–3

[16] Xu B Z, Li Z, Liu L L, Xu J, Chen C, Ning P P, Chen X L and Gu C Q 2015 Tunable band-notched coplanar waveguide based on localized spoof surface plasmons *Opt. Lett.* **40** 4683–6

[17] Li Z, Xu B Z, Liu L L, Xu J, Chen C, Gu C Q and Zhou Y J 2016 Localized spoof surface plasmons based on closed subwavelength high contrast gratings: concept and microwave-regime realizations *Sci. Rep.* **6** 27158

[18] Xu B Z, Li Z, Liu L L, Xu J, Chen C, Ning P P, Chen X L and Gu C Q 2016 Bandwidth tunable microstrip bandstop filters based on localized spoof surface plasmons *J. Opt. Soc. Am.* B **33** 1388–91

[19] Zhou Y J, Xiao Q X and Yang B J 2015 Spoof localized surface plasmons on ultrathin textured MIM ring resonator with enhanced resonances *Sci. Rep.* **5** 14819

[20] Yang B J, Zhou Y J and Xiao Q X 2015 Spoof localized surface plasmons in corrugated ring structures excited by microstrip line *Opt. Express* **23** 21434–42

[21] Pendry J B, Martin-Moreno L and Garcia-Vidal F J 2004 Mimicking surface plasmons with structured surfaces *Science* **305** 847–8

[22] Shen S, Cui T J, Martin-Cano D and Garcia-Vidal F J 2013 Conformal surface plasmons propagating on ultrathin and flexible films *Proc. Natl. Acad. Sci. USA* **110** 40–5

[23] Liu X, Feng Y, Chen K, Zhu B, Zhao J and Jiang T 2014 Planar surface plasmonic waveguide devices based on symmetric corrugated thin film structures *Opt. Express* **22** 20107–16

[24] Kianinejad A, Chen Z N and Qiu C W 2015 Design and modeling of spoof surface plasmon modes-based microwave slow-wave transmission line *IEEE Trans. Microw. Theory Tech.* **63** 1817–25

[25] Fernández-Domínguezf A I, Williams C R, Garcia-Vidal F J, Martin-Moreno L, Andrews S R and Maier S A 2008 Terahertz surface plasmon polaritons on a helically grooved wire *Appl. Phys. Lett.* **93** 141109

[26] Rüting F, Fernàndez-Domìnguezf A I, Martin-Moreno L F and Garcia- Vidal J 2012 Subwavelength chiral surface plasmons that carry tuneable orbital angular momentum *Phys. Rev.* B **86** 075437

[27] Liu L L, Li Z, Ning P P, Xu B Z, Chen C L, Xu J, Chen X L and Gu C Q 2015 Deep-subwavelength guiding and superfocusing of spoof surface plasmon polaritons on helically grooved metal wire *Plasmonics* **11** 359–64